A frequency-dependent effective medium model for the rheology of crystallizing polymers

Anthony Kotula

Materials Science and Engineering Division, NIST

Gaithersburg, MD 20899, United States

anthony.kotula@nist.gov

Abstract:

The rheology of crystallizing polymers is critical to polymer processing, but our current understanding of how crystallinity affects rheology during crystallization is lacking. The challenge is twofold: first, we must measure rheology simultaneously with crystallinity, and then we must develop models that can describe those measurements as well as prior phenomenological observations. Here, we further develop a generalized effective medium model to describe the frequency-dependent shear modulus of a crystallizing polymer. Through a simple model system, we show that the percolation transition in the effective medium model recovers the relaxation dynamics of a critical gel with a relaxation spectrum that can be approximated as the power mean of the initial melt and final semicrystalline material. We demonstrate the success of this model on the isothermal crystallization of polycaprolactones. From the generalized effective medium model, we can calculate the percolation fraction and power law relaxation exponent at the critical point, even when the measurement frequency range is dominated by shear thinning of the melt phase.

Introduction

Polymer crystallization is characterized by a dramatic structural and rheological transition from a homogeneous viscoelastic liquid to a hierarchically-structured solid. This solid state is comprised of ordered chain segments packed into crystalline lamellae interspersed with amorphous regions that contain loops, entanglements, and tie-chains that connect multiple crystalline regions. The mechanical properties of semicrystalline polymers are dictated by the crystalline microstructure and can be tuned with processing conditions that are imposed during the crystallization process. A better understanding of the mechanical properties during crystallization is therefore critical to controlling the final material properties of semicrystalline polymers used in injection molding,[1] film blowing,[2] fiber spinning,[3] or additive manufacturing.[4]

The first step to understanding the rheological properties of polymers crystallizing in highly dynamic, nonisothermal processes is to characterize the base case: quiescent isothermal crystallization of polymer melts. The viscoelastic response of a crystallizing polymer has been modeled using either empirical or phenomenological suspension-based relationships between the crystallinity and the complex shear modulus. The simplest empirical models relate the crystallinity to either the storage modulus[5] or the logarithm of the storage modulus[6]. Both are normalized such that the crystallinity varies from zero in the melt state to one in the semicrystalline state. Since the storage modulus can span multiple orders of magnitude during a crystallization process, the resulting crystallinity estimates from these models differ dramatically and should be treated with caution. Additionally, these models do not include any frequency dependence. Tanner treated the crystallizing polymer as a suspension of hard particles dispersed in the melt phase[7]. He reasoned that, in the limit of small strains and crystallinities, the crystallizing polymer can be treated as a dispersion of soft solid particles in a melt matrix. Therefore, the magnitude of the storage and loss moduli increase with increasing crystallinity, but frequency-dependent loss tangent does not change. Roozemond *et al*.[8] showed that the frequency dependence of the loss tangent varies with crystallinity for polyethylenes, and instead demonstrated that a self-consistent composite sphere model originally developed by Christensen and Lo[9] could capture the entire crystallization process over two decades in frequency.

Our more recent experiments could not successfully apply the model of Christensen and Lo to polycaprolactone crystallization.[10]

Other researchers have noted that crystallizing polymers exhibit a critical gel-like response at some point during the crystallization process. Pogodina and Winter first called attention to this phenomenon in polypropylenes,[11] noting a low-frequency plateau in the loss tangent which is characteristic of power-law relaxation dynamics. Their analysis describes the viscoelastic response of the partially-crystallized polymer but not the degree of crystallinity. The critical gel model has been used to characterize a number of crystallizing polymers,[12-16] but this material response is not captured by the current empirical or suspension-type models described above. Additionally, the determination of the loss tangent plateau is challenging, since the "true" critical loss tangent can occur in a frequency range well below that used in a rheology measurement during crystallization.[17]

Experimental measurements have been made on a number of polymers to develop and test models relating crystallinity to rheology.[8, 10-12, 18-23] Since rheology cannot directly measure crystallinity, separate measurements of viscoelasticity and crystallinity are performed and correlated under similar thermal conditions. Correlations between rheology and separate crystallinity measurements via light scattering,[24] optical microscopy,[25] differential scanning calorimetry (DSC),[20, 26] or wide-angle X-ray scattering[27] are challenging due to the sensitive dependence of crystallization kinetics on the thermal and mechanical history of the sample. This problem has been addressed through the development of instrumentation capable of simultaneous rheology and crystallinity measurements. Nuclear magnetic resonance[28] and DSC[29] instruments have been coupled to rheometers to measure the volume average crystallinity of the entire sample. These methods are currently unable to perform spatially-resolved crystallinity measurements which are critical to understanding the crystallization process. Spatial measurements of crystallinity can be obtained through optical microscopy using a transparent rheometer base, where the focal point can be positioned radially (from the plate center to the edge) and axially (from the lower plate to the upper tool).[22] Spatial mapping of the spherulite size and position provides a measurement of the degree of space filling, however these techniques are limited to low crystallinities due

to light scattering from overlapping spherulites. Roy *et al*. recently extended this method to larger degrees of space filling by combining experiments with numerical simulations.[23] This method is practical when the nucleation rate of spherulites is small relative to the growth rate such that a countable number of spherulites can be measured. Polymers with high nucleation density cannot be characterized optically.

To address these measurement challenges we developed a measurement technique for simultaneous rheology, optical microscopy, and Raman spectroscopy called the rheo-Raman microscope.[30] Raman spectroscopy is sensitive to single chain conformation as well as inter-chain interactions that occur when chains are packed into a crystalline configuration. It can therefore be used to determine pre-crystalline chain ordering during isothermal crystallization[31] or the presence of dipole-dipole interactions in the melt state.[32] These spectra can also be correlated with quantitative crystallinity measurements, generally via DSC, to convert features in the Raman spectrum to crystallinity during crystallization.[32] Raman spectroscopy can be focused using simple optical elements; in the rheo-Raman microscope, we are able to measure the Raman spectrum using the same optical objective that is used for reflection-mode optical microscopy.

We have used the rheo-Raman microscope to assess models relating crystallinity to rheology in polycaprolactone.[10] Our measurements of the shear modulus and crystallinity showed that neither empirical models nor suspension-based models could describe isothermal crystallization. We instead developed a generalized effective medium (GEM) model that phenomenologically describes crystallization as a percolation-type process. The model includes two scaling parameters (s and t) that account for the sensitivity of the modulus to increasing amounts of crystalline material near the crystallinity where critical percolation occurs. We found that by setting $s = t$, we could adequately describe the relationship between the shear modulus and crystallinity at a single frequency. This model has also been successful in characterizing the crystallization process in polymer nanocomposites[33] and isotactic polypropylene[23]. Roy *et al*. noted a gap-dependent relationship between the modulus and crystallinity due to the growth of spherulitic clusters or “superstructures” that grew to span the rheometer gap. Under conditions where the

gap is large relative to the individual spherulites comprising the spanning superstructure, the crystallization process follows a gap-independent percolation process consistent with the GEM model.

Here, we extend the applicability of the GEM model to characterize the crystallinity-modulus relationship over a wide range of frequencies spanning at least two orders of magnitude. We first analyze the GEM model at the critical percolation fraction to show that the model predicts percolation, then we use a simple model viscoelastic system to show how the GEM model compares to the critical gel model of Winter[11]. We find that the power law critical gel response can be observed when the measurement frequencies are well within the terminal response of the zero-crystallinity polymer melt. Combined Raman spectroscopy and rheology measurements on two crystallizing polycaprolactones are used to develop crystallinity-modulus curves over two orders of magnitude in frequency. The GEM model with non-equal scaling exponents is used to fit the experimental results, and we determine the critical percolation fraction even when the plateau in the loss tangent occurs well outside the experimental measurement range.

Theory

The GEM model predicts the complex modulus $G^*(\omega)$ at a given crystallinity ξ as [10]

$$(1-\xi)\frac{\left(G_0^*(\omega)\right)^{1/s}-\left(G^*(\omega)\right)^{1/s}}{\left(G_0^*(\omega)\right)^{1/s}+A\left(G^*(\omega)\right)^{1/s}}+\xi\frac{\left(G_\infty^*(\omega)\right)^{1/t}-\left(G^*(\omega)\right)^{1/t}}{\left(G_\infty^*(\omega)\right)^{1/t}+A\left(G^*(\omega)\right)^{1/t}}=0 \qquad (1)$$

where the complex shear modulus of the initial polymer melt with zero crystallinity ($\xi=0$) is $G_0^*(\omega)$ and the complex modulus once the polymer has reached the semicrystalline state ($\xi=1$) is $G_\infty^*(\omega)$. The parameter $A=(1-\xi_c)/\xi_c$ where ξ_c is the critical volume fraction where percolation occurs, and so *A* can range from 0 (at ξ_c = 1) to infinity (at ξ_c = 0). The exponents *s* and *t* describe the modulus scaling on either side of the percolation transition, where below percolation $G^* \sim (\xi_c-\xi)^{-s}$ and above percolation $G^* \sim (\xi-\xi_c)^t$. When $\xi<\xi_c$, the GEM model describes an effective medium comprised of structures with semicrystalline modulus dispersed in a melt matrix, and above the percolation transition the equation

describes melt inclusions dispersed in a semicrystalline matrix. The applicability of equation (1) was discussed in our previous work [10] for modulus measurements at a single frequency $\omega = 2\pi$ rad/s and equal exponents $s = t$.

At the percolation condition $\xi = \xi_c$, the GEM model predicts a critical modulus $G_c^*(\omega)$ that is given by the nonlinear equation

$$\left(\frac{G_c^*(\omega)}{G_0^*(\omega)}\right)^{1/s}\left(\frac{G_c^*(\omega)}{G_\infty^*(\omega)}\right)^{1/t} - \frac{A-1}{A}\left(\frac{G_c^*(\omega)}{G_\infty^*(\omega)}\right)^{1/t} - \frac{1}{A} = 0 \ . \tag{2}$$

The critical modulus cannot be determined analytically for arbitrary values of the moduli and GEM parameters, however an approximation is possible. Comparing the first two terms in eq (2) suggests that we can neglect the second term under conditions where $\left(G_c^*/G_0^*\right)^{1/s} >> (A-1)/A$. For values of the percolation fraction $\xi_c < 0.66$ the second term coefficient falls within the range $-1 < (A-1)/A < 1$. All previously measured values of the percolation fraction fall well within this range[10, 23, 33]. Under conditions where $\left(G_c^*/G_0^*\right)^{1/s}$ is at least an order of magnitude larger than $(A-1)/A$ we can treat the second term in eq (2) as negligible to approximate the critical shear modulus as

$$G_c^*(\omega) \approx \left(\frac{1}{A}\right)^{ns}\left(G_0^*(\omega)\right)^n\left(G_\infty^*(\omega)\right)^{1-n} \tag{3}$$

where we have introduced a power law index $n = t/(s+t)$. The critical modulus $G_c^*(\omega)$ is therefore proportional to a power mean [34] of the melt modulus and the semicrystalline modulus when eq (3) is valid. We note that the relative magnitude of the scaled modulus ratio $\left(G_c^*/G_0^*\right)^{1/s}$ will vary over the frequency range, whereas the function $(A-1)/A$ is a constant. Therefore, eq (3) might only be valid within a low frequency range or for low modulus materials. Generally, the valid frequency range for eq (3) will depend on the viscoelastic spectrum of the melt and semicrystalline states and the shape of the semicrystalline domains which will affect ξ_c.

The implications of frequency-dependent moduli on the GEM model are easily demonstrated by an analytical example of a Maxwell fluid crystallizing into an ideal elastic solid. The Maxwell fluid has a well-known frequency dependence

$$G_M^*(\omega) = G_{M,0}\frac{(\tau_M\omega)^2}{1+(\tau_M\omega)^2} + iG_{M,0}\frac{\tau_M\omega}{1+(\tau_M\omega)^2} \tag{4}$$

which is characterized by a high frequency plateau modulus $G_{M,0}$ and a timescale τ_M. The zero-shear viscosity of the Maxwell fluid is the product of the plateau modulus and the relaxation timescale, $\eta_M = G_{M,0}\tau_M$. The elastic solid has a constant value of the shear modulus independent of the oscillation frequency

$$G_E^* = G_{E,0} \ . \tag{5}$$

It is straightforward to substitute eqs (4) and (5) into eq (1) and calculate the complex shear modulus at different crystallinities. We assume modulus values comparable to those of polymers in the melt and semicrystalline state: for the Maxwell fluid we set the high frequency plateau $G_{M,0} = 10^6$ Pa and the elastic solid modulus $G_{E,0} = 10^9$ Pa. The characteristic timescale of the Maxwell fluid is set to $\tau_M = 1$ s.

Figure 1 shows the frequency dependence of the storage and loss moduli for the Maxwell material crystallizing into an elastic solid for arbitrary values of *s*, *t*, and ξ_c. Note that we have chosen parameters such that the assumptions used to generate eq (3) are valid over the frequency range. There is a monotonic increase in both the storage and loss moduli as the crystallinity increases up to the critical percolation fraction (Figure 1a). As the crystallinity increases beyond the percolation transition (Figure 1b), the storage and loss moduli continue to increase, however at higher crystallinities the loss modulus sharply drops to zero (not shown on a logarithmic scale) due to the ideal elastic solid model used for the solid phase. The storage modulus shows a plateau at lower frequencies when $\xi > \xi_c$, which indicates that the material has transitioned from a viscoelastic liquid to a solid. The storage and loss moduli at the critical percolation

fraction are parallel with a power law frequency dependence at lower angular frequencies. There is good agreement between the GEM model (eq (1)) and the approximation at the critical percolation threshold (eq (3)). Using eq (3), we find that the low-frequency limit at the percolation threshold for this case is

$$\lim_{\omega\to 0} G_c^*(\omega) = \frac{G_{E,0}^{1-n}\eta_M^n}{A^{ns}}\omega^n\left[\cos\left(\frac{\pi}{2}n\right)+i\sin\left(\frac{\pi}{2}n\right)\right], \tag{6}$$

which indicates that the storage and loss moduli are indeed parallel at low frequencies with a power-law index $n = t/(s+t)$. Equation (6) indicates that the modulus at percolation consists of a storage modulus $G_c' = \left(G_{E,0}^{1-n}\eta_M^n / A^{ns}\right)\cos(\pi n/2)\omega^n$ and a loss modulus $G_c'' = \left(G_{E,0}^{1-n}\eta_M^n / A^{ns}\right)\sin(\pi n/2)\omega^n$ at low frequencies.

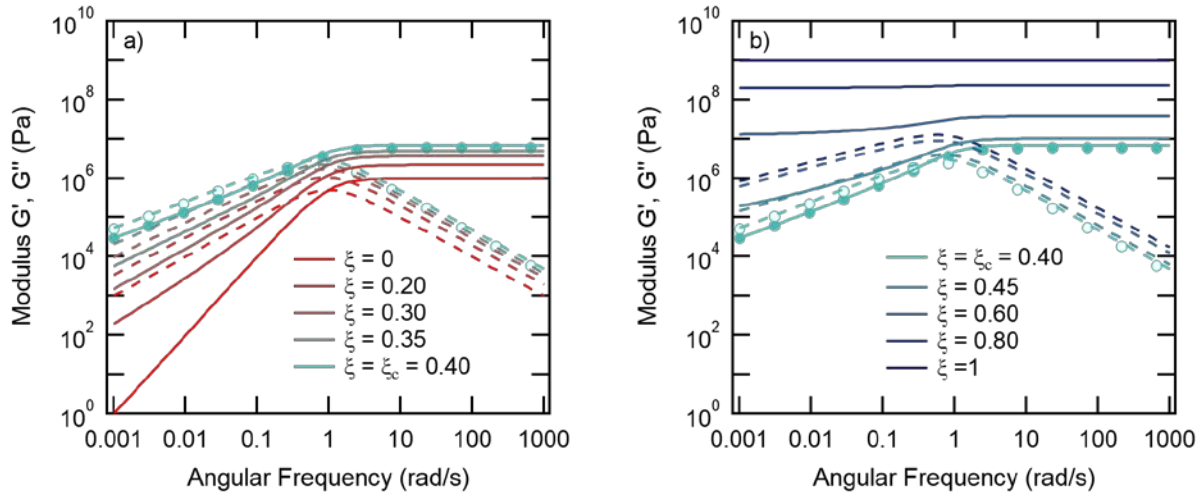

Figure 1. Shear modulus versus frequency for a Maxwell fluid crystallizing into an elastic solid calculated from eq (1). *G*' is shown by the solid lines, *G*" is shown by the dashed lines. a) Crystallinities below the percolation threshold $\xi_c = 0.40$. b) Crystallinities above the percolation threshold. The symbols indicate the values of *G*' (●) and *G*" (○) at the critical percolation fraction as estimated from eq (3). The scaling exponents are $s = 2$ and $t = 4$.

We can further visualize the effect of crystallinity on the viscoelastic spectrum of the ideal crystallizing system via the loss tangent (tan δ) as shown in Figure 2. Small amounts of crystallinity have a more pronounced effect on the loss tangent at low frequencies until the critical percolation fraction is

reached. We can calculate the low-frequency loss tangent at the percolation condition from eq (6). Recalling that $\tan\delta = G''/G'$, we can estimate the critical loss tangent at the percolation fraction tan δ_c as

$$\lim_{\omega\to 0}\tan\delta_c = \frac{G_c''}{G_c'} = \tan\left(\frac{\pi}{2}n\right). \tag{7}$$

Beyond the percolation fraction, the loss tangent drops precipitously as the crystallizing material approaches a purely elastic response. We note that tan δ_c starts to deviate from the frequency-independent plateau at frequencies that are approximately one to two orders of magnitude less than $1/\tau_M$.

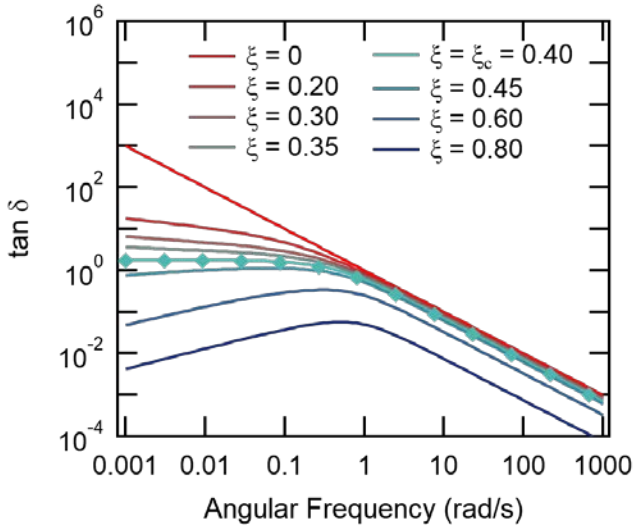

Figure 2. Loss tangent versus frequency for a Maxwell fluid crystallizing into an elastic solid calculated from eq (1). The symbols indicate the values of tan δ_c at the critical percolation fraction as estimated from eq (3).

The viscoelastic response predicted in eqs (6) and (7) exhibits a similar frequency dependence to the critical gel model initially developed by Chambon and Winter[35] for chemically crosslinking systems at the gel point, which was later used to analyze the crystallization process in polypropylene.[11] The critical gel model is characterized by the gel stiffness S and an exponent n_w such that in small-amplitude oscillatory shear, the sample exhibits a complex shear modulus which we can write as

$$G_{cw}^*(\omega) = S\Gamma(1-n_w)(i\omega)^{n_w} \quad \text{for } 0<\omega<1/\lambda_0 \tag{8}$$

where Γ is the gamma function and λ_0 is a characteristic timescale where additional relaxation processes cause the shear modulus to deviate from the power-law dependence. A direct comparison of eqs (6) and (8) indicates that the GEM model exponent n is equivalent to n_w, and the gel stiffness S is a function of the power law index n_w, the material properties characterizing the viscoelastic properties of the melt and semicrystalline states, and the critical percolation fraction. In the example of the Maxwell material crystallizing to an elastic solid,

$$S = \frac{1}{\Gamma(1-n)} \frac{G_{E,0}}{A^{ns}} \left(\frac{\eta_M}{G_{E,0}} \right)^n . \tag{9}$$

Within the GEM model, we find that the gel stiffness has a non-negligible dependence on the critical percolation fraction embedded in A. This contrasts with the approximation made by Izuka *et al*. for the stiffness of a *chemical* gel at the critical point,[36] which posits the stiffness as $S = G_0 \left(\eta_0 / G_0 \right)^{n_w}$ where G_0 is the modulus of the fully crosslinked material and η_0 is the zero-shear viscosity of the prepolymer. The approximation of Izuka *et al.*[36] fails when applied to the *physical* gelation process in crystallizing isotactic polypropylene.[11]

Experimental

Two commercial grades of poly-ε-caprolactone (PCL) were received in pellet form from Perstorp and used as received (see Disclaimer). We will refer to the grades as “PCL97” and “PCL162” respectively. Gel permeation chromatography measurements were performed on the polymer dissolved in tetrahydrofuran and were calibrated at 30 °C using narrow-dispersity polystyrene standards. PCL97 has a mass-average molar mass of 96.6 kg/mol and a dispersity of 1.77, and PCL162 has a mass-average molar mass of 161.6 kg/mol and a dispersity of 1.90. The uncertainty on the molar mass measurements is 10%.

Pellets are melt-pressed at 100 °C for 5 minutes to form 1 mm thick disks that are loaded into a rheo-Raman microscope (Thermo Fisher) [30]. The 8 mm parallel-plate upper geometry is lowed to a trimming height of 700 μm, the sample is trimmed, and the gap is lowered to a measurement height of 600 μm. The sample is then held for 5 minutes at 100 °C (which is well above the equilibrium melt temperature

of 69 °C [37]); this annealing temperature is known to completely remove melt memory effects in PCL after 3 minutes in DSC experiments.[38] After annealing, the sample is cooled to a crystallization temperature T_c by first cooling at a rate of 10 °C/min to (T_c + 5) °C, then immediately cooling at a rate of 2 °C/min to T_c. Oscillatory measurements are performed at the crystallization temperature via frequency sweeps in a "controlled strain" mode in the range of 1 rad/s to 100 rad/s and a strain of 0.004.

Raman measurements are performed using a 532 nm laser at a power of 10 mW focused approximately 9.5 mm from the center of the plate using a 5x objective. Four five-second exposures are averaged together for each Raman spectrum. Crystallinity measurements are performed by analyzing the C=O stretch region of the Raman spectrum using methods developed previously. [10, 32] The C=O stretch region (1600 cm^{-1} to 1850 cm^{-1}) is fit using three basis spectra attributed to different chain conformers: a crystalline chain conformation with a peak at 1722 cm^{-1}, an amorphous random coil conformation at 1735 cm^{-1}, and an amorphous conformation with dipole-dipole interactions at 1727 cm^{-1}.[32] The shapes of the basis spectra are not standard Gaussian, Lorentzian, or Voight shapes but are determined from self modeling curve resolution.[39] During fitting the peak shapes and relative peak positions are fixed, and the three basis spectra intensities and one horizontal shift factor (common to all three basis spectra) are used to fit the experimental spectrum. The integrated intensity of the crystalline basis spectra I_C relative to the total integrated intensity of the three basis spectra I_T is related to the mass fraction crystallinity α_c via the relationship $\alpha_c = 1.26\ I_C/I_T$, where the numerical constant was determined by linear regression.[32] The maximum relative error in α_c from this equation is 2%.

Results

Material Characterization

The melt rheology results are shown in Figure 3. The storage and loss moduli are measured over a frequency range of 1 rad/s to 100 rad/s at temperatures ranging from 55 °C to 175 °C (in increments of 15 °C). Although the lowest measurement temperatures are below the equilibrium melt temperature, no crystallinity is observed in the sample via Raman spectroscopy or the polarized optical microscope attachment on the instrument. The data are horizontally shifted to a reference temperature of 100 °C using the "Automatic TTS Shift" procedure in RepTate.[40] The shift factors a_T follow an Arrhenius-type temperature dependence

$$a_T\left(T\right) = \exp\left[\frac{E_a}{R}\left(\frac{1}{T} - \frac{1}{T_0}\right)\right] \tag{10}$$

where E_a is the activation energy, R is the gas constant, and T_0 is the reference temperature (100 °C). The activation energies for PCL97 and PCL167 are (31.4 ± 0.9) kJ/mol and (30.8 ± 0.7) kJ/mol in agreement with prior measurements of PCL melts.[41-43] The activation energy calculations are included in the Supplementary Material.

The linear viscoelasticity shown in Figure 3 indicates longer relaxation timescales for the higher molar mass sample, with a crossover in G' and G'' occurring near 40 rad/s. The lower molar mass sample does not exhibit a crossover in the angular frequency range probed and shows terminal relaxation behavior at frequencies below 1 rad/s. The viscoelasticity of both samples can be fit using a multimode Maxwell model

$$G^* = \sum_{k=1}^{N} G_k \frac{\left(\omega\tau_k\right)^2}{1+\left(\omega\tau_k\right)^2} + iG_k \frac{\omega\tau_k}{1+\left(\omega\tau_k\right)^2} \tag{11}$$

with modulus G_k and characteristic relaxation timescale τ_k for the k^{th} mode. The best fit values of the modulus and characteristic timescale for each mode are given in Table I. Since terminal behavior is not observed for PCL162, we expect that longer relaxation timescales are necessary to characterize the full

viscoelastic response of this sample in the melt state. Complete characterization of the viscoelastic spectrum is not required for our current purpose.

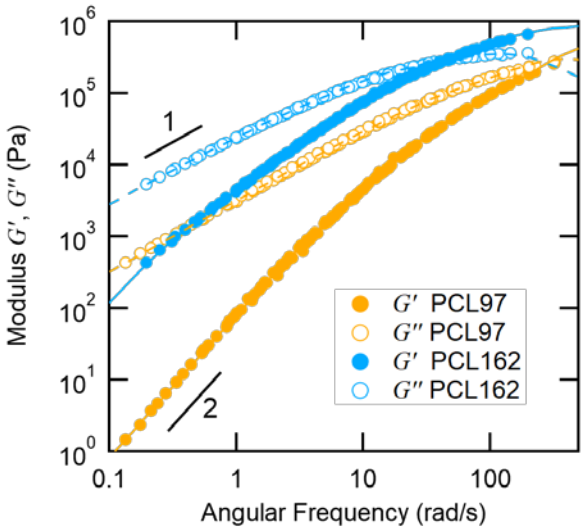

Figure 3. Melt rheology of the PCL samples at a reference temperature of 100 °C. The lines are fits to a generalized Maxwell model, with coefficients shown in Table I. Power law slopes of 1 and 2 are indicated.

Table 1. Maxwell modes for melt rheology at 100 °C.

	PCL97		PCL162	
k	G_k (Pa)	τ_k (s)	G_k (Pa)	τ_k (s)
1	$(1.32 \pm 0.36) \times 10^3$	$(2.1 \pm 0.2) \times 10^{-1}$	$(1.71 \pm 0.22) \times 10^3$	2.3 ± 0.2
2	$(4.45 \pm 0.56) \times 10^4$	$(3.1 \pm 0.4) \times 10^{-2}$	$(2.23 \pm 0.16) \times 10^4$	$(3.4 \pm 0.3) \times 10^{-1}$
3	$(4.53 \pm 0.21) \times 10^5$	$(4.6 \pm 0.4) \times 10^{-3}$	$(2.31 \pm 0.11) \times 10^5$	$(5.1 \pm 0.4) \times 10^{-2}$
4	-	-	$(6.40 \pm 0.13) \times 10^5$	$(7.6 \pm 0.5) \times 10^{-3}$

Isothermal Crystallization

The results of simultaneous rheology and crystallinity measurements are shown in Figure 4 for PCL97. A small increase in the moduli occurs during the first 400 s, which is most noticeable in the low frequency *G*' results. We attribute this increase to thermal equilibration of the sample that occurs after the instrument achieves the isothermal crystallization temperature. This thermal equilibration timescale is confirmed using a poly(phenylmethylsiloxane) (Gelest) subjected to the same temperature profile (see Supplementary Material). An initial nonzero offset in the crystallinity of approximately 0.02 is observed, which is the noise threshold for crystallinity measurements using our fitting procedure. Both the

crystallinity and the moduli increase during the crystallization process. The crossover in the storage and loss moduli at frequencies of 1 rad/s and 10 rad/s occur when the polymer melt is at approximately 15% crystallinity by mass. The moduli at the highest frequency exhibit no such crossover since *G*'(100 rad/s) is always greater than *G*"(100 rad/s). At times greater than 3000 s both the moduli and the crystallinity slowly increase with time due to a secondary crystallization process.[10, 27]

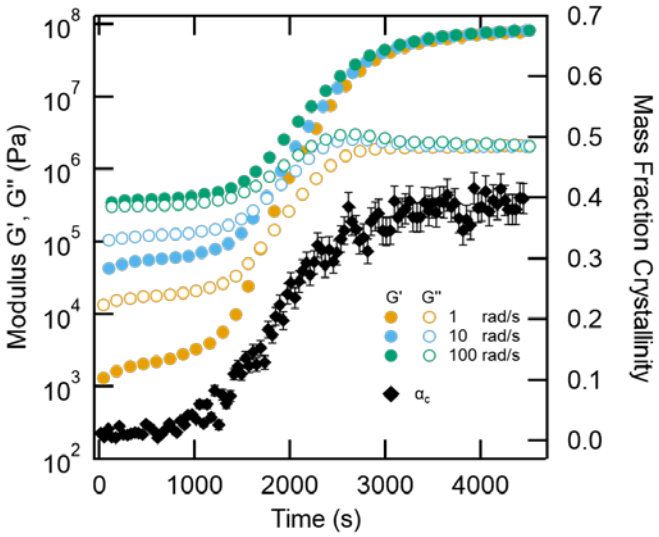

Figure 4. Viscoelasticity and crystallinity measurements of PCL97 during isothermal crystallization at 44 °C. Moduli at three frequencies are shown for clarity.

The simultaneous measurements allow us to describe the frequency-dependent modulus as a function of crystallinity. We first smooth the crystallinity data using a 5-point moving average to reduce noise, then interpolate the crystallinity to the times when the moduli were measured. The resulting modulus-crystallinity plot is shown in Figure 5. The thermal equilibration at early times is now evident through the increase in the modulus at crystallinity values less than 0.02, followed by an increase in both G′ and G″ with increasing crystallinity. There is an inflection point in the loss modulus at mass fraction crystallinities slightly greater than 0.3, which becomes less evident at lower frequencies.

In order to fit the GEM model to the data shown in Figure 5, we must convert the mass fraction crystallinity α_c to a relative volume fraction of crystallinity ξ. We do this by first calculating the volume fraction $\phi = \alpha_c / \left(\alpha_c + \left(\nu_m / \nu_c\right)\left(1-\alpha_c\right)\right)$ based on the specific volumes of the melt phase ν_m and the

crystal phase v_c. We then scale the volume fraction by the volume fraction ϕ_∞ where spherulites have filled the sample volume, which we determine using a linear regression method described previously.

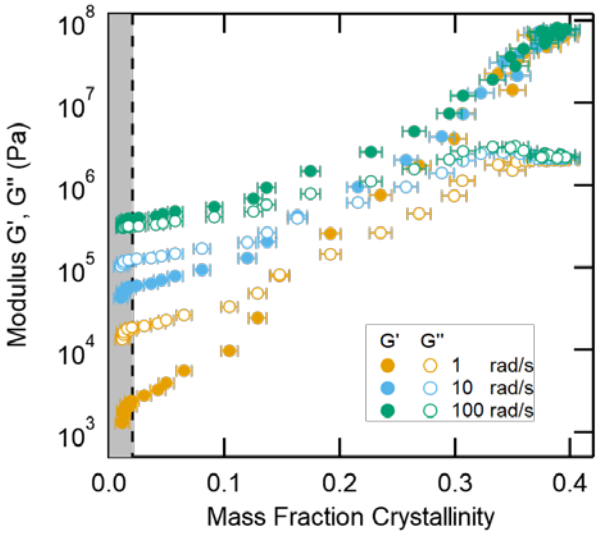

Figure 5. Results from Figure 4 plotted with the modulus as a function of mass fraction crystallinity. Symbols are the same as in Figure 4. Horizontal error bars indicate uncertainty in mass fraction crystallinity. The grey region bound by the vertical dashed line indicates crystallinity values below the noise threshold of 0.02.

The GEM model given by eq (1) fits both the storage and loss moduli over two orders of magnitude in frequency for single values of *s*, *t*, and ξ_c as shown in Figure 6a. Here, we set the zero crystallinity value of the complex modulus $G_0^*(\omega)$ to be the first oscillatory measurement performed where the crystallinity first exceeds 0.02 for each frequency and the semicrystalline complex modulus $G_\infty^*(\omega)$ where $\xi = 1$. The critical percolation fraction from the GEM model occurs around a relative crystallinity of 0.37, which results in a mass fraction crystallinity of approximately 0.15. This is well within the range of percolation fractions measured previously for this material.[10] Figure 6b indicates that the model also exhibits acceptable agreement with the magnitude of tan δ over the range of frequencies and crystallinities. Unlike previous applications of the GEM model,[10, 23, 33] *s* is not set equal to *t*. The value of *s* is less than 2 but is still within the range of 1.5 – 2 expected for the viscosity of particle suspensions.[44, 45] This agrees with our prior application of the GEM model at a single frequency. The scaling exponent *t* is significantly

larger than 2 and outside the range of exponents calculated for some model porous ceramics[46] but the values are well within the range of values observed for various porous materials (ranging from 1 to approximately 7).[47]

The model also captures the inflection point in G'' that is observed at relative crystallinities slightly greater than 0.8 (or mass fractions greater than 0.3 in Figure 5) for frequencies greater than 10 rad/s. We note that, after inflection, the loss modulus decreases with increasing crystallinity until volume is filled with spherulites. This part of the crystallization process is well-described by a continuous semicrystalline matrix with dispersed viscoelastic melt domains. We also note from Figure 6b that the loss tangent is more sensitive to increasing amounts of crystallinity above relative crystallinities of 0.8, and the higher frequency measurements exhibit a steeper slope in tan δ with increasing crystallinity. Although a complete mathematical description is beyond the scope of this work, previous theoretical modeling on two-phase viscoelastic composites has shown that composites can have a loss modulus that exceeds both the loss modulus of the matrix or the inclusion for a given frequency.[48, 49] The observation of this maximum is a function of the melt and semicrystalline moduli as well as the two-phase microstructure described by s, t, and ξ_c. The inflection does not indicate an additional structural transition in the crystallizing polymer.

Examining the GEM model results in more detail in Figure 6b we observe that the low-frequency tan δ values display a crossover near a relative crystallinity of 0.45. This crossover is often used to estimate the gel point of crystallizing polymers,[50] but the critical percolation fraction calculated from the GEM model occurs at a lower relative crystallinity. We can attribute the discrepancy to melt relaxation processes occurring over the frequency range used to measure the shear modulus. If we extrapolate the longest relaxation time for PCL97 to 42 °C using the Arrhenius relationship shown in eq (10), then the expected frequency range is within the longest melt relaxation timescale of 1.5 s. Thus, we expect shear thinning of the melt phase to affect the frequency dependence of loss tangent during the crystallization process. Our examination of the GEM model in the Theory section suggests that the plateau in tan δ at the gel point would only be observed at frequencies two orders of magnitude below the inverse of the longest relaxation timescale, which for the results shown in Figures 4 – 6 would be below 10^{-2} rad/s.

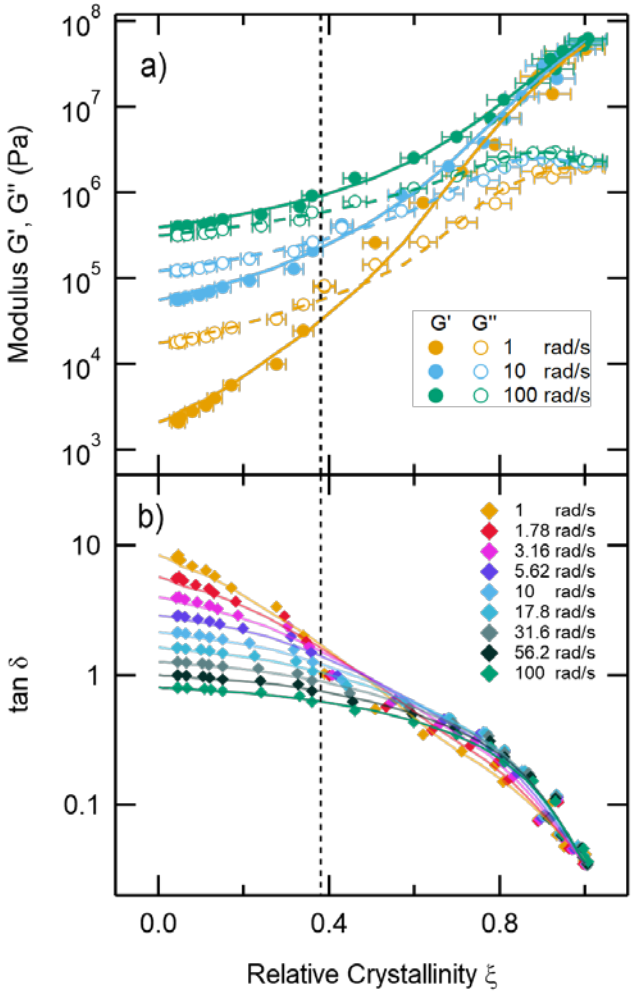

Figure 6. Results from Figure 4 plotted as a) modulus versus relative crystallinity with the GEM model fit for G' (solid lines) and G'' (dashed lines), and b) tan δ versus relative crystallinity for all measured angular frequencies with the GEM model fit shown with solid lines. The GEM model parameters are $s = 1.50 \pm 0.14$, $t = 5.45 \pm 0.94$, and $\xi_c = 0.38 \pm 0.08$. The dashed vertical line indicates the critical percolation fraction. Horizontal error bars indicate uncertainty due to uncertainty propagation of the mass fraction crystallinity and are not included in (b) for clarity.

The GEM model also performs well when applied to materials with longer melt relaxation timescales, as shown in Figure 7 for PCL162. An extrapolation of the relaxation timescales to the crystallization temperature using the Arrhenius relationship indicates that the longest relaxation timescale is approximately 15 s, and therefore our oscillatory measurements in the range of 1 rad/s to 100 rad/s are probing well into the shear-thinning regime of the melt phase. Despite this, the GEM model can again fit

the experimental results remarkably well for single values of *s*, *t*, and ξ_c. The crossover in the lowest frequency tan δ values occurs at relative crystallinities in the range of 0.5 – 0.6, which is much greater than the critical percolation fraction from the GEM model. Extrapolating the longest measured relaxation timescale from Table 1 to the crystallization temperature suggests that the plateau in tan δ would be observable at frequencies less than 10^{-3} rad/s. The values of *s* and *t* are again commensurate with the scaling parameters for the viscosity of particle suspensions and the modulus of porous materials, respectively.

The values of the fitting exponents are insensitive to temperature over the narrow range of 42 °C to 46 °C, as shown in Figure 8. Within this temperature range, the scaling exponents and percolation fraction are largely independent of temperature and molecular weight, with one exception being the decrease in *t* for PCL162 with increasing crystallization temperature. The exponent *t* is sensitive to the geometry of the melt domains interspersed between semicrystalline domains once the sample has crystallized beyond the percolation transition. Higher values of the scaling exponent *t* generally occur in porous materials comprised of overlapping spheres as in cases of sintered powders.[46, 47] Ascribing a strict geometric description to the value of *t* in porous materials is not possible, but values of approximately 4 or greater are associated with more anisotropic, interconnected pore geometries.[47] These values are consistent with an interconnected, anisotropic melt domain that would be formed from the random growth of spherulites during the crystallization process. The decrease in *t* for PCL162 at higher temperatures indicates that the viscoelastic melt domains after percolation are less interconnected than the melt domains in crystallization processes that occur at slightly lower temperatures. Although the fitting parameters are similar for PCL97 and PCL162 over the temperature range, attempts to fit all modulus-crystallinity measurements to a single set of fitting parameters proved unsuccessful.

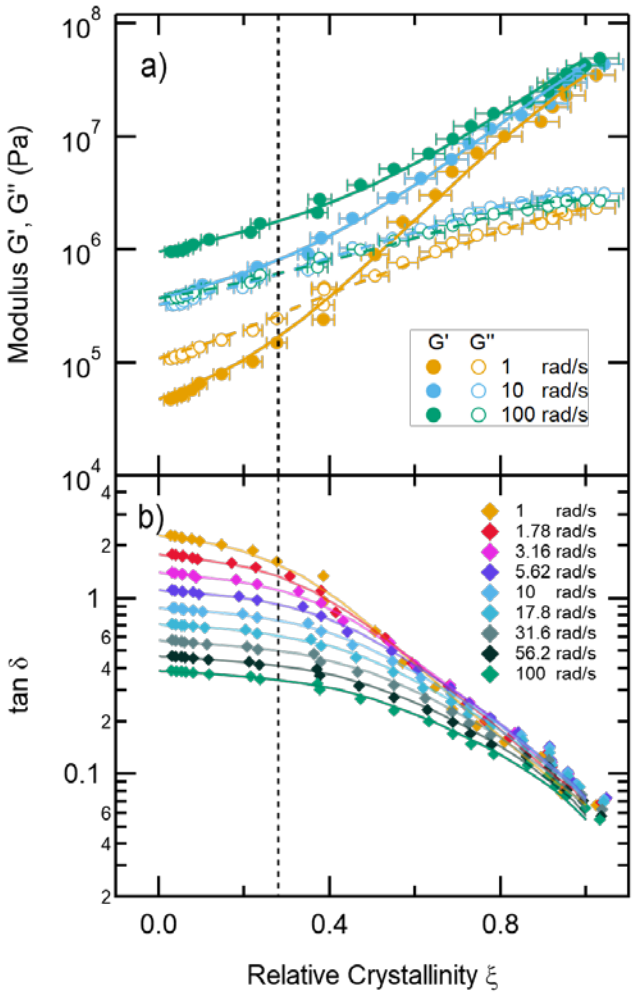

Figure 7. Isothermal crystallization of PCL162 at 42 °C. a) Modulus versus relative crystallinity with the GEM model fit for G' (solid lines) and G'' (dashed lines), reported at 1 rad/s, 10 rad/s, and 100 rad/s. Symbols are the same as in Figure 4. b) tan δ versus relative crystallinity for all measured angular frequencies with the GEM model fit shown with solid lines. The GEM model parameters are $s = 1.79 \pm 0.26$, $t = 4.60 \pm 1.21$, and $\xi_c = 0.28 \pm 0.16$. The dashed vertical line indicates the critical percolation fraction. Horizontal error bars indicate uncertainty due to uncertainty propagation of the mass fraction crystallinity and are not included in (b) for clarity.

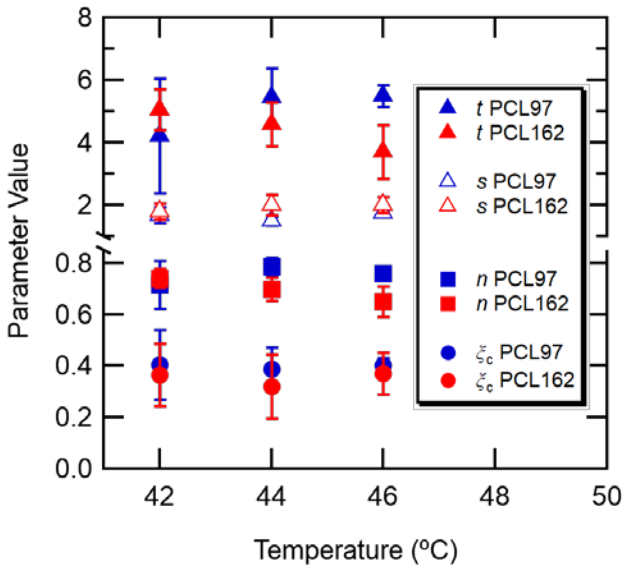

Figure 8. GEM model parameters at different isothermal crystallization temperatures. Error bars indicate the standard deviation of three measurements.

Based on the values of *s* and *t*, the scaling exponent at the percolation condition *n* is found in the range $0.6 < n < 0.8$. This indicates that the partially crystalline polycaprolactone acts like a "soft" gel ($n > 0.5$) at the critical point.[11] Prior crystallization measurements performed on a crystallizing polycaprolactone have been analyzed using the gelation model, and the resulting n_w values occur between 0.6 and 0.8 with an average value of 0.73.[14] The agreement between the measured *n* values from the GEM model and the n_w values indicates that the GEM model at the critical percolation point can capture the important characteristics of Winter's gelation model.

Figure 8 shows that the two polycaprolactones have the same average percolation fraction over the temperature range. Although the percolation fraction can vary significantly between individual experiments (compare the percolation fraction in Figures 6 and 7), the value of the percolation fraction consistently occurs at relative crystallinities in the range of approximately 0.3 to 0.5. These values are above the geometrical percolation threshold for overlapping monodisperse spheres (0.2895).[51] Since the geometrical percolation threshold always precedes the mechanical percolation threshold,[52] values of $\xi_c > 0.29$ are consistent with the growth and impingement of spherical structures. Polydispersity in the sphere

size distribution would shift the percolation threshold to higher values;[53] for polymer crystallization, we would therefore expect the heterogeneous nucleation of spherulites to percolate at volume fractions closer to 0.3 and homogeneous nucleation processes to percolate at higher volume fractions. Since the critical (mechanical) percolation fraction in Figure 8 generally occurs at higher volume fractions, the mechanical percolation transition occurs due to a connected network of disperse spherulite sizes that have spanned the rheometer gap. Small gap sizes in rheometers are known to shift the percolation threshold to lower crystallinities,[23] which are not observed here. The variability in the percolation fraction indicates the sensitivity of the mechanical percolation process to the microstructure formed during the crystallization process. We note that the critical percolation fractions measured from these rheo-Raman measurements are larger than the crystallinities calculated at the gel point for crystallizing PCL samples characterized using separate rheology and DSC measurements.[14]

Our results show that the relationship between rheology and crystallinity is well-explained by the GEM model. The model provides an adequate fit to experimental results using single values of the critical percolation fraction ξ_c and critical exponents *s* and *t*, even when the rheological measurements are performed outside the frequency range where a terminal response is observed. For polycaprolactone, the fitting parameters are well-described by the growth and percolation of semicrystalline spherulites from the polymer melt.

Discussion

The GEM model describes a very simple picture of the crystallization process: semicrystalline spherulites of a constant viscoelasticity grow within a polymer melt of constant viscoelasticity. The spherulites initially act as solid particle filler in a melt matrix until the spherulites form a percolating network capable of supporting stress, and beyond this point the melt domains act as low modulus filler dispersed in a semicrystalline matrix. Although the model is phenomenological, it provides a relatively straightforward relationship between modulus and crystallinity that can be applied in continuum modeling during crystallization processes.

Although the GEM model parameters are similar for the isothermal, quiescent crystallization processes studied here, different semicrystalline structures will have a significant effect on the scaling exponents and percolation fraction. One important case is when shish-kebab structures are generated in flow – from the composites-based approach taken in this work, we expect that some concepts used to predict the properties of fiber-polymer composites will be applicable to predicting the rheological properties of flow-induced crystallization.[54-56] The percolation fraction will be affected by both the aspect ratio of the fiber-like shish structures as well as their orientation. If the flow strongly orients the shish to be parallel to the rheometer plates we would expect a higher percolation fraction than that of spherulites; however, if the shish are not well-oriented (due to reorientation during or after flow) the percolation could occur at relative crystallinities well below that for spherulites. Composite theory often treats the shear modulus G of a fiber composite with fibers of modulus G_f and volume fraction ϕ oriented parallel to the flow direction as an "inverse mixing rule" described by Reuss [57]: $G^{-1} = \phi / G_f + (1-\phi) / G_m$, where G_m is the modulus of the fluid matrix. We can recover the Reuss model from eq (1) when $s = t = 1$ and the critical percolation fraction approaches 1; therefore, we expect the highly-aligned shish-kebab morphology to decrease both s and t from the values shown in Figure 8. Cases where the alignment is reduced will yield scaling factors that are sensitive to the orientation distribution and are outside the scope of this work.

One significant assumption is that the melt phase and semicrystalline spherulites have constant relaxation spectra during the crystallization process. Polymer melts with broad molecular weight distributions are known to reject low molecular weight chains from the crystal.[58] This fractionation would bias the molar mass distribution towards the shorter chains and therefore change the relaxation spectrum of the melt phase. Semicrystalline spherulites are known to exhibit secondary thickening processes during crystallization wherein lamellae continue to thicken and new crystal lamellae are formed within the amorphous domains of the growing spherulite.[59, 60] We should therefore consider the spherulite a composite of amorphous and crystalline domains and expect the effective modulus of the spherulite to increase when secondary crystallization occurs. Given this reality, it is surprising that the GEM model performs as well as shown here for constant values of the melt and semicrystalline states. Application of the GEM model to a broad range of polymers and molar mass distributions will help to further refine our model to describe the rheology of the crystallization process.

The rheology of the crystallization process can also be dependent upon the measurement geometry as shown by Roy, Audus, and Migler.[23] They found that the crystallinity-modulus relationship for polymers with a low nucleation density (like isotactic polypropylene) would be subject to finite-size effects where a small number of spherulites span the gap in a parallel-plate geometry. Although the GEM model can be used to fit the results, the resulting fitting parameters are a function of the microstructure and the measurement geometry. We can estimate whether finite-size effects are affecting our measurements on PCL via the dimensionless nucleation rate $\dot{N}_{\mathrm{b}}^{'} = \dot{N}_{\mathrm{b}} h^4 / v_{\mathrm{s}}$ where $\dot{N}_{\mathrm{b}}$ is the nucleation rate per unit volume, h is the gap height, and v_{s} is the spherulite growth rate. Measurements of the nucleation and growth rates of PCL in a temperature range of 46 °C to 51 °C suggest nucleation rates of order 10^{10} $\mathrm{m^{-3}s^{-1}}$ and growth rates of order 10^{-8} m/s,[61] and with a gap of 6×10^{-4} m the dimensionless nucleation rate is $\dot{N}_{\mathrm{b}}^{'} \approx 10^5$, well above the criteria $\dot{N}_{\mathrm{b}}^{'} > 1000$ required to neglect finite-size effects.

Conclusions

The general effective medium model successfully describes the relationship between crystallinity and the complex shear modulus over a wide range of angular frequencies. The critical percolation fraction and scaling exponents indicate that the effective modulus of crystallizing polymers can be treated as suspensions with high modulus semicrystalline particles growing and eventually forming a percolating network throughout the sample. This concept appears valid even at measurement frequencies comparable to the timescales of relaxation processes in the melt phase. Thus, we can determine the critical percolation fraction and scaling exponents without having to measure the terminal response of the crystallizing polymer. Our model predicts that the modulus at the critical percolation condition can be approximated as a power mean of the moduli of the pure melt and semicrystalline phases in certain cases.

Our results show that a simple model can be used to describe the relationship between crystallinity and the rheology of crystallizing polymers. We expect this model to be useful in characterizing the mechanical properties of polymers with enhanced crystallization kinetics due to shear flow. The model greatly simplifies the crystallization process by assuming that both phases have a constant viscoelastic response; however, a reality of time- or crystallinity- dependent viscoelasticity for the melt and semicrystalline phases is more likely. Our results motivate further experimental and theoretical assessment of the crystallization process to better understand the relationship between morphology and the rheological percolation process. This modulus-crystallinity relationship will be useful in continuum modeling of polymer processing techniques including film-blowing and the additive manufacturing of semicrystalline polymers.

Acknowledgements

The author would like to thank Sara Orski for performing gel permeation chromatography measurements and Kalman Migler for helpful discussions.

Supplementary Material

See Supplementary Material for further information on the activation energy calculation from melt rheology and the thermal equilibration timescale measurements of poly(phenylmethylsiloxane).

Disclaimer

Certain commercial equipment, instruments, or materials are identified in this paper in order to adequately specify experimental procedure. Such identification does not imply recommendation or endorsement by the National Institute of Standards and Technology, nor does it imply that the materials or equipment identified are necessarily the best available for the purpose.

[1] Katti, S. S., and Schultz, M., ‘‘The microstructure of injection-molded semicrystalline polymers: A review,’’ Polymer Engineering & Science **22**, 1001-1017 (1982).
[2] Doufas, A. K., and McHugh, A. J., ‘‘Simulation of film blowing including flow-induced crystallization,’’ Journal of Rheology **45**, 1085-1104 (2001).
[3] van Meerveld, J., Hütter, M., and Peters, G. W. M., ‘‘Continuum model for the simulation of fiber spinning, with quiescent and flow-induced crystallization,’’ Journal of Non-Newtonian Fluid Mechanics **150**, 177-195 (2008).
[4] McIlroy, C., Seppala, J. E., and Kotula, A. P., “Combining Modeling and Measurements To Predict Crystal Morphology in Material Extrusion.” *Polymer-Based Additive Manufacturing: Recent Developments* (American Chemical Society, 2019).
[5] Gauthier, C., Chailan, J.-F., and Chauchard, J., ‘‘Utilisation de l'analyse viscoélastique dynamique à l'étude de la cristallisation isotherme du poly(téréphtalate d'ethylène) amorphe. Application à des composites unidirectionnels avec fibres de verre,’’ Die Makromolekulare Chemie **193**, 1001-1009 (1992).
[6] Pogodina, N. V., Winter, H. H., and Srinivas, S., ‘‘Strain effects on physical gelation of crystallizing isotactic polypropylene,’’ Journal of Polymer Science Part B: Polymer Physics **37**, 3512-3519 (1999).
[7] Tanner, R. I., ‘‘On the flow of crystallizing polymers: I. Linear regime,’’ Journal of Non-Newtonian Fluid Mechanics **112**, 251-268 (2003).
[8] Roozemond, P. C., Janssens, V., Van Puyvelde, P., and Peters, G. W. M., ‘‘Suspension-like hardening behavior of HDPE and time-hardening superposition,’’ Rheologica Acta **51**, 97-109 (2012).
[9] Christensen, R. M., and Lo, K. H., ‘‘Solutions for effective shear properties in three phase sphere and cylinder models,’’ Journal of the Mechanics and Physics of Solids **27**, 315-330 (1979).
[10] Kotula, A. P., and Migler, K. B., ‘‘Evaluating models for polycaprolactone crystallization via simultaneous rheology and Raman spectroscopy,’’ Journal of Rheology **62**, 343-356 (2018).
[11] Pogodina, N. V., and Winter, H. H., ‘‘Polypropylene Crystallization as a Physical Gelation Process,’’ Macromolecules **31**, 8164-8172 (1998).
[12] Coppola, S., Acierno, S., Grizzuti, N., and Vlassopoulos, D., ‘‘Viscoelastic Behavior of Semicrystalline Thermoplastic Polymers during the Early Stages of Crystallization,’’ Macromolecules **39**, 1507-1514 (2006).
[13] Acierno, S., Grizzuti, N., and Winter, H. H., ‘‘Effects of Molecular Weight on the Isothermal Crystallization of Poly(1-butene),’’ Macromolecules **35**, 5043-5048 (2002).
[14] Acierno, S., Di Maio, E., Iannace, S., and Grizzuti, N., ‘‘Structure development during crystallization of polycaprolactone,’’ Rheologica Acta **45**, 387-392 (2006).

[15] Horst, R. H., and Winter, H. H., ‘‘Stable critical gels of a crystallizing copolymer of ethene and 1-butene,’’ Macromolecules **33**, 130-136 (2000).
[16] Gelfer, Y., and Winter, H. H., ‘‘Effect of Branch Distribution on Rheology of LLDPE during Early Stages of Crystallization,’’ Macromolecules **32**, 8974-8981 (1999).
[17] Schwittay, C., Mours, M., and Winter, H. H., ‘‘Rheological expression of physical gelation in polymers,’’ Faraday Discussions **101**, 93-104 (1995).
[18] Khanna, Y. P., ‘‘Rheological mechanism and overview of nucleated crystallization kinetics,’’ Macromolecules **26**, 3639-3643 (1993).
[19] Boutahar, K., Carrot, C., and Guillet, J., ‘‘Crystallization of polyolefins from rheological measurements relation between the transformed fraction and the dynamic moduli,’’ Macromolecules **31**, 1921-1929 (1998).
[20] Carrot, C., Guillet, J., and Boutahar, K., ‘‘Rheological behavior of a semi-crystalline polymer during isothermal crystallization,’’ Rheologica acta **32**, 566-574 (1993).
[21] Ratzsch, K.-F., Friedrich, C., and Wilhelm, M., ‘‘Low-field rheo-NMR: A novel combination of NMR relaxometry with high end shear rheology,’’ Journal of Rheology **61**, 905-917 (2017).
[22] Pantani, R., Speranza, V., and Titomanlio, G., ‘‘Simultaneous morphological and rheological measurements on polypropylene: Effect of crystallinity on viscoelastic parameters,’’ Journal of Rheology **59**, 377-390 (2015).
[23] Roy, D., Audus, D. J., and Migler, K. B., ‘‘Rheology of crystallizing polymers: The role of spherulitic superstructures, gap height, and nucleation densities,’’ Journal of Rheology **63**, 851-862 (2019).
[24] Pogodina, N. V., Siddiquee, S. K., van Egmond, J. W., and Winter, H. H., ‘‘Correlation of Rheology and Light Scattering in Isotactic Polypropylene during Early Stages of Crystallization,’’ Macromolecules **32**, 1167-1174 (1999).
[25] Pogodina, N. V., Lavrenko, V. P., Srinivas, S., and Winter, H. H., ‘‘Rheology and structure of isotactic polypropylene near the gel point: quiescent and shear-induced crystallization,’’ Polymer **42**, 9031-9043 (2001).
[26] Titomanlio, G., Speranza, V., and Brucato, V., ‘‘On the simulation of thermoplastic injection moulding process: II Relevance of interaction between flow and crystallization,’’ International Polymer Processing **12**, 45-53 (1997).
[27] Steenbakkers, R. J. A., and Peters, G. W. M., ‘‘Suspension-based rheological modeling of crystallizing polymer melts,’’ Rheologica Acta **47**, 643 (2008).
[28] Räntzsch, V., Özen, M. B., Ratzsch, K.-F., Stellamanns, E., Sprung, M., Guthausen, G., and Wilhelm, M., ‘‘Polymer Crystallization Studied by Hyphenated Rheology Techniques: Rheo-NMR, Rheo-SAXS, and Rheo-Microscopy,’’ Macromolecular Materials and Engineering **0**, 1800586 (2018).
[29] Janssens, V., Block, C., Van Assche, G., Van Mele, B., and Van Puyvelde, P., ‘‘RheoDSC: design and validation of a new hybrid measurement technique,’’ Journal of Thermal Analysis and Calorimetry **98**, 675 (2009).
[30] Kotula, A. P., Meyer, M. W., Vito, F. D., Plog, J., Walker, A. R. H., and Migler, K. B., ‘‘The rheo-Raman microscope: Simultaneous chemical, conformational, mechanical, and microstructural measures of soft materials,’’ Review of Scientific Instruments **87**, 105105 (2016).
[31] Migler, K. B., Kotula, A. P., and Hight Walker, A. R., ‘‘Trans-Rich Structures in Early Stage Crystallization of Polyethylene,’’ Macromolecules **48**, 4555-4561 (2015).
[32] Kotula, A. P., Snyder, C. R., and Migler, K. B., ‘‘Determining conformational order and crystallinity in polycaprolactone via Raman spectroscopy,’’ Polymer **117**, 1-10 (2017).
[33] Roy, D., Kotula, A. P., Natarajan, B., Gilman, J. W., Fox, D. M., and Migler, K. B., ‘‘Effect of cellulose nanocrystals on crystallization kinetics of polycaprolactone as probed by Rheo-Raman,’’ Polymer **153**, 70-77 (2018).
[34] Bulletin, P. S., *Handbook of Means and Their Inequalities Vol. 560* (Kluwer Academic Publishers, The Netherlands, 2003).

[35] Chambon, F., and Winter, H. H., ‘‘Linear Viscoelasticity at the Gel Point of a Crosslinking PDMS with Imbalanced Stoichiometry,’’ Journal of Rheology **31**, 683-697 (1987).
[36] Izuka, A., Winter, H. H., and Hashimoto, T., ‘‘Molecular weight dependence of viscoelasticity of polycaprolactone critical gels,’’ Macromolecules **25**, 2422-2428 (1992).
[37] Lebedev, B., and Yevstropov, A., ‘‘Thermodynamic properties of polylactones,’’ Die Makromolekulare Chemie **185**, 1235-1253 (1984).
[38] Lorenzo, A. T., and Müller, A. J., ‘‘Estimation of the nucleation and crystal growth contributions to the overall crystallization energy barrier,’’ Journal of Polymer Science Part B: Polymer Physics **46**, 1478-1487 (2008).
[39] Lawton, W. H., and Sylvestre, E. A., ‘‘Self modeling curve resolution,’’ Technometrics **13**, 617-633 (1971).
[40] Ramirez, J., and Likhtman, A.E., *Rheology of Entangled Polymers: Toolbox for the Analysis of Theory and Experiments* (Reptate, https://reptate.readthedocs.io/, 2018)
[41] Noroozi, N., Thomson, J. A., Noroozi, N., Schafer, L. L., and Hatzikiriakos, S. G., ‘‘Viscoelastic behaviour and flow instabilities of biodegradable poly (ε-caprolactone) polyesters,’’ Rheologica Acta **51**, 179-192 (2012).
[42] Kelly, C. A., Murphy, S. H., Leeke, G. A., Howdle, S. M., Shakesheff, K. M., and Jenkins, M. J., ‘‘Rheological studies of polycaprolactone in supercritical CO2,’’ European Polymer Journal **49**, 464-470 (2013).
[43] Sangroniz, L., Barbieri, F., Cavallo, D., Santamaria, A., Alamo, R. G., and Müller, A. J., ‘‘Rheology of self-nucleated poly(ε-caprolactone) melts,’’ European Polymer Journal **99**, 495-503 (2018).
[44] Denn, M. M., and Morris, J. F., ‘‘Rheology of Non-Brownian Suspensions,’’ Annual Review of Chemical and Biomolecular Engineering **5**, 203-228 (2014).
[45] Wildemuth, C. R., and Williams, M. C., ‘‘Viscosity of suspensions modeled with a shear-dependent maximum packing fraction,’’ Rheologica Acta **23**, 627-635 (1984).
[46] Roberts, A. P., and Garboczi, E. J., ‘‘Elastic Properties of Model Porous Ceramics,’’ Journal of the American Ceramic Society **83**, 3041-3048 (2000).
[47] Ji, S., Gu, Q., and Xia, B., ‘‘Porosity dependence of mechanical properties of solid materials,’’ Journal of Materials Science **41**, 1757-1768 (2006).
[48] Gibiansky, L. V., and Lakes, R., ‘‘Bounds on the complex bulk modulus of a two-phase viscoelastic composite with arbitrary volume fractions of the components,’’ Mechanics of Materials **16**, 317-331 (1993).
[49] Milton, G. W., and Berryman, J. G., ‘‘On the effective viscoelastic moduli of two–phase media. ii. rigorous bounds on the complex shear modulus in three dimensions,’’ Proceedings of the Royal Society of London. Series A: Mathematical, Physical and Engineering Sciences **453**, 1849-1880 (1997).
[50] Holly, E. E., Venkataraman, S. K., Chambon, F., and Henning Winter, H., ‘‘Fourier transform mechanical spectroscopy of viscoelastic materials with transient structure,’’ Journal of Non-Newtonian Fluid Mechanics **27**, 17-26 (1988).
[51] Rintoul, M. D., and Torquato, S., ‘‘Precise determination of the critical threshold and exponents in a three-dimensional continuum percolation model,’’ Journal of Physics A: Mathematical and General **30**, L585-L592 (1997).
[52] Bicerano, J., Douglas, J. F., and Brune, D. A., ‘‘Model for the Viscosity of Particle Dispersions,’’ Journal of Macromolecular Science, Part C **39**, 561-642 (1999).
[53] Lorenz, B., Orgzall, I., and Heuer, H. O., ‘‘Universality and cluster structures in continuum models of percolation with two different radius distributions,’’ Journal of Physics A: Mathematical and General **26**, 4711-4722 (1993).
[54] Ramazani SA, A., Ait-Kadi, A., and Grmela, M., ‘‘Rheology of fiber suspensions in viscoelastic media: Experiments and model predictions,’’ Journal of Rheology **45**, 945-962 (2001).
[55] Laun, H., ‘‘Orientation effects and rheology of short glass fiber-reinforced thermoplastics,’’ Colloid and Polymer Science **262**, 257-269 (1984).

[56] Metzner, A. B., ‘‘Rheology of Suspensions in Polymeric Liquids,’’ Journal of Rheology **29**, 739-775 (1985).
[57] Reuss, A., ‘‘Berechnung der Fließgrenze von Mischkristallen auf Grund der Plastizitätsbedingung für Einkristalle,’’ ZAMM - Journal of Applied Mathematics and Mechanics / Zeitschrift für Angewandte Mathematik und Mechanik **9**, 49-58 (1929).
[58] Mehta, A., and Wunderlich, B., ‘‘A study of molecular fractionation during the crystallization of polymers,’’ Colloid and Polymer Science **253**, 193-205 (1975).
[59] Akpalu, Y., Kielhorn, L., Hsiao, B. S., Stein, R. S., Russell, T. P., van Egmond, J., and Muthukumar, M., ‘‘Structure Development during Crystallization of Homogeneous Copolymers of Ethene and 1-Octene: Time-Resolved Synchrotron X-ray and SALS Measurements,’’ Macromolecules **32**, 765-770 (1999).
[60] Kolb, R., Wutz, C., Stribeck, N., von Krosigk, G., and Riekel, C., ‘‘Investigation of secondary crystallization of polymers by means of microbeam X-ray scattering,’’ Polymer **42**, 5257-5266 (2001).
[61] Chynoweth, K. R., and Stachurski, Z. H., ‘‘Crystallization of poly(ε-caprolactone),’’ Polymer **27**, 1912-1916 (1986).